Polymer 49 (2008) 4808–4818

Contents lists available at ScienceDirect

Polymer

journal homepage: www.elsevier.com/locate/polymer

Polymer–filler interaction in nanocomposites: New interface area function to investigate swelling behavior and Young's modulus

Mithun Bhattacharya, Anil K. Bhowmick*

Rubber Technology Center, Indian Institute of Technology, Kharagpur, West Bengal 721302, India

ARTICLE INFO

Article history:
Received 6 March 2008
Received in revised form 1 September 2008
Accepted 2 September 2008
Available online 12 September 2008

Keywords:
Nanocomposites
Polymer–filler interaction
Interface area function

ABSTRACT

Polymer–filler interaction for nanocomposites was quantified by introducing Interface Area Function (IAF), to account for the nanofiller characteristics comprising of the specific surface area, correlation length and the filler volume fraction. IAF supplants the immeasurable filler characteristic terms, rendering tractability to the equation derived by considering the restraining forces acting on a nanofiller-elliptical platelet-embedded in polymer matrix. However, neglecting such terms reduces the same to Kraus's equation. Recognition of the due importance of such filler characteristics, by introduction of IAF, resulted in better fitment of swelling data and also conformance with the trend predicted by Zisman's interpretation of surface energy. Experimental values of Young's modulus of natural rubber and styrene–butadiene rubber nanocomposites and those predicted by Guth–Gold and Halpin–Tsai equations for composites conform post-introduction of IAF, with mere 5–20% deviations. The accurate fitment of the resulting constitutive equations indicates suitable integration of the shape and aggregate effects.

1. Introduction

The degree of crosslink density in vulcanized elastomeric gum compounds can be estimated by applying the Flory–Rehner network theory [1]. But their extrapolation into the domain of filled compounds presents certain theoretical and practical complications, prime among them being the restriction to deformation in proportion with the sample dimension. These restrictive forces arise from the presence of the rigid inclusions engrafted in the rubber matrix.

Bueche [2], Kraus [3] and Boonstra and Dannenberg [4] have separately studied this problem to come up with the understanding that although strong theoretical reasons cannot be assigned, the apparent crosslink density from equilibrium swelling data accounts for the polymer–filler interaction. This has established that swelling experimentation on filled compounds yields a measure of the physical crosslinking in elastomeric compounds.

The observations of Lorenz and Parks [5] have led to the conclusion that the swelling of bulk rubber is essentially the same in both the filled and the unfilled compounds and the effect of the inclusion is predominantly felt in the interfacial region only. Within this region, the restriction to swelling is maximum due to adherence of rubber to filler by means of adsorption. On moving radially outwards from the filler, which is the epicenter of the restraining forces, the effect subsides and beyond a certain imaginary sphere of influence, the rubber swells to the same extent as the bulk of the gum compound. This swelling model was effectively utilized by Kraus [6] to quantize the effect on swelling exerted by bonded spherical particles in rubber matrices.

Although the swelling in the case of polymer nanocomposites (PNCs) agrees in principle with this, it undervalues the importance of the extended interface offered by the change in filler shape and aggregate characteristics. Literature search indicates that the suitability of the Kraus plot to platelet-like nanofillers has not been investigated. In the present work, we evaluate the same and attempt to extend it to the domain of PNCs by incorporating certain modifications. The extra terms that evolve on application of "the swelling of the rubber shell" approach to the platelet filler are represented by an interface area function (IAF). This function maps the shape and aggregate effects, characteristic of nanofillers, to accurately determine the polymer–filler interaction in PNCs. Since the polymer–filler interaction has direct consequence on the modulus, the derived function is subjected to validation by introducing the function in established models for determination of composite modulus.

Some earlier reports dealing with the micromechanics of the intercalated or exfoliated polymer–clay nanocomposites [7–9] have attempted to understand the reinforcing mechanism of polymer-layered silicate nanocomposites. In our earlier communications [10–15], on clay and silica nanocomposites we have attempted to correlate the reinforcement with swelling behavior in terms of the volume fraction of rubbers. It appears that there is a gap in the

* Corresponding author. Tel.: +91 3222 283180; fax: +91 3222 220312.
E-mail address: anilkb@rtc.iitkgp.ernet.in (A.K. Bhowmick).

0032-3861/$ – see front matter © 2008 Elsevier Ltd. All rights reserved.
doi:10.1016/j.polymer.2008.09.002

literature on this subject. Thus, in this paper, apart from investigating the swelling behavior, we also address the superior reinforcing efficiency of rubber nanocomposites by introducing the new interface area function into the composite theories proposed by Guth and Gold [16], Guth [17] and Halpin and Tsai [18,19].

The reinforcing effect of spherical colloidal fillers on elastomers was studied by Guth and Gold [16], who obtained the following equation.

$$E = E_m\left[1 + 2.5\phi + 14.1\phi^2\right] \quad (1)$$

Guth [17] later modified the above equation by introducing a shape factor α (length/breadth) in order to account for the accelerated stiffening at higher loadings, considering that the aggregate structures of spherical fillers resemble rod-like filler particles embedded in a continuous matrix. Guth, thus, arrived at the modified Guth–Gold equation,

$$E = E_m\left[1 + 0.67\alpha\phi + 1.62(\alpha\phi)^2\right] \quad (2)$$

The elastic modulus of composite materials reinforced by discontinuous cylindrical fibers or lamellar shapes is expressed by the Halpin–Tsai equations [18,19], as shown in the following equation.

$$E = E_m\left\{\frac{1 + \xi\eta\phi}{1 - \eta\phi}\right\} \quad (3)$$

where, $\xi = 2\alpha$ and $\eta = \left[(E_f/E_m) - 1\right]/\left[(E_f/E_m) + \xi\right]$.

However, at high filler concentration, the predicted value of Eq. (3) does not agree with the experimental data [20], due to the exclusion of several important factors in Eq. (3).

1.1. Theory

For determination of the restriction to swelling offered by adhering filler, Kraus considered a filler particle of radius R engrafted in a matrix of rubber. The rubber is assumed to swell, whereas the filler is an inextensible body. It is further presumed that the polymer–nanofiller interaction is strong enough to withstand the interfacial stresses generated due to swelling. Thus, as the rubber swells, with the rubber–filler bond remaining intact, a consequential restriction to swelling is registered.

Since the nanofillers, particularly the nanoclays, have different structures, the model generated with spherical filler as the restraining body is inexpedient. Thus, we consider the entrapment of a non-expansible elliptical filler (with eccentricity ε) within the rubber matrix (Fig. 1).

In polar coordinates, an ellipse with one focus at the origin and the other on the negative x-axis is represented by the general equation $r(1 + \varepsilon\cos\theta) = l$, where l is the semi-latus rectum of the ellipse. Thus, analogous to the spherical filler of radius R in the Kraus model, we consider an elliptical filler given by $R(1 + \varepsilon\cos\theta)$, in the polar coordinate. The swelling is completely restricted at the surface and the restriction diminishes radially outwards (Fig. 1). This restriction is experienced till the hypothetical sphere of influence of the restraining filler is existent. We can designate r_{app} ($>R(1 + \varepsilon\cos\theta)$) as a certain distance away from the center of the particle where the restriction is still being felt and as the distance approaches infinity, the swelling assumes normality, as in a gum compound. This distance r_{app}, however, is not a fixed or well defined point in space and in fact is variable and is conceived to extend till the outer surface of the hypothetical sphere of influence.

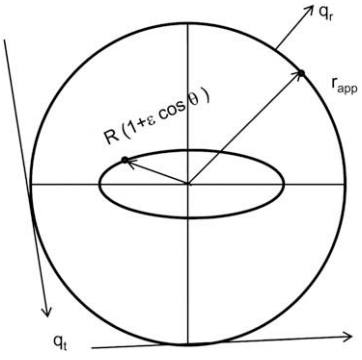

Fig. 1. Elliptical nanofiller embedded in a rubber matrix.

Any volume element in the unswelled rubber can be represented, in terms of polar coordinates, as dr, $r\,d\theta$, $r\sin\theta\,d\psi$. Post-swelling this element will assume the dimension of $q_r\,dr$, $q_t r\,d\theta$, $q_t r\sin\theta\,d\psi$, where q is a function of r. From the requirement of solid angle conservation, the tangential (q_t) and the radial (q_r) components of the linear expansion coefficient (q_0) must differ. Furthermore, to be able to derive the volume swelling deficiency caused by each restraining particle we need to be able to relate these two quantities.

Also, the distance by which the elemental volume gets displaced from the center of the particle (r'), post-swelling, is

$$r' = \int_{R(1+\varepsilon\cos\theta)}^{r_{app}} q_r dr + R(1 + \varepsilon\cos\theta) \quad (4)$$

Because of the requirement,

$$r'\,d\theta = q_t r\,d\theta \quad (5)$$

we have,

$$q_t r - R(1 + \varepsilon\cos\theta) = \int_{R(1+\varepsilon\cos\theta)}^{r_{app}} q_r\,dr \quad (6)$$

Differentiating with respect to 'r',

$$q_r = q_t + r(dq_t/dr) \quad (7)$$

This equation suitably relates the radial (q_r) and the tangential (q_t) components of the linear expansion coefficient (q_0).

Now, if we are to assume that the rubber swells equally in all directions, even in the presence of the filler, the swollen volume in the presence of filler is

$$\int_0^{2\pi}\int_0^{\pi}\int_{R(1+\varepsilon\cos\theta)}^{r_{app}} q_r q_t^2 r^2\sin\theta\,dr\,d\theta\,d\psi \quad (8)$$

This is the annular volume enclosed between the top surface of the filler, extending radially till the upper limit of the hypothetical sphere of influence (Fig. 1). The lower limit is thus set to $R(1 + \varepsilon\cos\theta)$. The assumption that the rubber swells equally in all directions can be safely incorporated, because the farther one moves away from the surface, the lesser is the restriction imposed and in such circumstances the subsiding extent of influence is better represented by a sphere than an ellipsoid. Also, in the absence of any restraining media the swollen volume of the element would have been

$$\iiint q_0^3 r^2\sin\theta\,dr\,d\theta\,d\psi \quad (9)$$

Thus, if we consider that the sphere of influence exists till r_{app}, the swelling deficiency will be felt within a shell of rubber bound between $R(1 + \varepsilon\cos\theta)$ and r_{app}. This can be equated to the difference of expressions (8) and (9), which implies that the swelling deficiency per particle, Δv, is

$$\Delta v = \int_0^{2\pi}\int_0^{\pi}\int_{R(1+\varepsilon\cos\theta)}^{r_{app}} \left(q_r q_t^2 - q_0^3\right) r^2 \sin\theta \, dr \, d\theta \, d\psi \quad (10)$$

Using Eq. (7) in Eq. (10), we have

$$\Delta v = \int_0^{2\pi}\int_0^{\pi}\int_{R(1+\varepsilon\cos\theta)}^{r_{app}} \left[\{q_t + r(dq_t/dr)\}q_t^2 - q_0^3\right] \times r^2 \sin\theta \, dr \, d\theta \, d\psi \quad (11)$$

Integrating with respect to $d\psi$ over the limits,

$$\Delta v = 2\pi \int_0^{\pi}\int_{R(1+\varepsilon\cos\theta)}^{r_{app}} \left[\{q_t + r(dq_t/dr)\}q_t^2 - q_0^3\right] r^2 \sin\theta \, dr \, d\theta \quad (12)$$

But, the following identity can be used to evaluate the integral:

$$r^2 q_t^3 + r^3 q_t^2 (dq_t/dr) = 1/3\left[d\left(r^3 q_t^3\right)/dr\right]$$

such that Eq. (12) simplifies to

$$\Delta v = 2\pi \int_0^{\pi}\int_{R(1+\varepsilon\cos\theta)}^{r_{app}} \left[\frac{1}{3}\frac{d}{dr}\left(r^3 q_t^3\right) - q_0^3 r^2\right] dr \sin\theta \, dr \, d\theta \quad (13)$$

Now, integrating with respect to dr for the radial component and passing on the limits, we get,

$$\Delta v = 2\pi \int_0^{\pi} \left\{\frac{1}{3} r_{app}^3 q_t^3 - \frac{1}{3} R^3 (1+\varepsilon\cos\theta)^3 q_t^3 - \frac{q_0^3}{3}\left[r_{app}^3 - R^3(1+\varepsilon\cos\theta)^3\right]\right\} \sin\theta \, d\theta$$

Since there can be no swelling at the lower limit, which is the filler surface, q_t at lower limit is unity. Replacing for that, we have,

$$\Delta v = 2\pi \int_0^{\pi} \left\{\frac{1}{3} r_{app}^3 q_t^3(r) - \frac{1}{3} R^3 (1+\varepsilon\cos\theta)^3 \cdot 1 - \frac{q_0^3}{3}\left[r_{app}^3 - R^3(1+\varepsilon\cos\theta)^3\right]\right\} \sin\theta \, d\theta$$

On rearranging, the swelling deficiency is

$$\Delta v = 2\pi \int_0^{\pi} \left\{\frac{1}{3} r_{app}^3 q_t^3(r) - \frac{1}{3} R^3 (1+\varepsilon\cos\theta)^3 \left(1 - q_0^3\right) - \frac{q_0^3 r_{app}^3}{3}\right\} \sin\theta \, d\theta$$

$$\Delta v = \frac{2\pi}{3} \int_0^{\pi} \left[\left\{r_{app}^3\left\{q_t^3(r) - q_0^3\right\} - R^3\left(1 - q_0^3\right)\left(1 + 3\varepsilon\cos\theta + 3\varepsilon^2\cos^2\theta + \varepsilon^3\cos^3\theta\right)\right] \sin\theta \, d\theta$$

Now, integrating with respect to $d\theta$, we arrive at the equation

$$\Delta v = \frac{2\pi}{3}\left[\left\{-r_{app}^3\left\{q_t^3(r) - q_0^3\right\}\cos\theta\right]_0^{\pi}\right\} + R^3(1 - q_0^3) \times \left\{\cos\theta + \frac{3\varepsilon\cos^2\theta}{2} + \varepsilon^2\cos^3\theta + \frac{\varepsilon^3\cos^4\theta}{4}\right\}\Bigg]_0^{\pi}$$

On introducing the limits, it reduces to

$$\Delta v = \frac{2\pi}{3}\left[-r_{app}^3\left\{q_t^3(r) - q_0^3\right\}(-2) + R^3\left(1 - q_0^3\right)\left(-2 - 2\varepsilon^2\right)\right]$$

or,

$$\Delta v = \frac{4\pi}{3}\left[r_{app}^3\left\{q_t^3(r) - q_0^3\right\} + R^3\left(q_0^3 - 1\right)\left(1 + \varepsilon^2\right)\right]$$

Taking $R^3 q_0^3$ out as the common factor and rearranging,

$$\Delta v = \frac{4\pi q_0^3 R^3}{3}\left[\left(1 - 1/q_0^3\right)\left(1 + \varepsilon^2\right) + \frac{r_{app}^3\{q_t^3(r)/q_0^3 - 1\}}{R^3}\right] \quad (14)$$

For us to determine the precise value of the swelling deficiency, the term q_t needs to be resolved into a physically tangible quantity. Striving to achieve that we realize that at the filler surface restriction to swelling is maximum and it reduces as we traverse radially outwards. As a consequence, at the filler surface the expansion is least and the expansion coefficient q_t is unity. Hence, the linear swelling coefficient is such a function of (r) that

$$f(\infty) = 0$$

and

$$f\{R(1+\varepsilon\cos\theta)\} = 1.$$

Thus, q_t can be represented as,

$$q_t = q_0 - (q_0 - 1)f(r) \quad (15)$$

Using Eq. (15) in Eq. (14) and passing the limits,

$$\Delta v = \frac{4\pi q_0^3 R^3}{3}\left[\left(1 - 1/q_0^3\right)\left(1 + \varepsilon^2\right) + \frac{\lim_{r\to\infty} r_{app}^3\left[(q_t^3/q_0^3) - 1\right]}{R^3}\right] \quad (16)$$

Also, the function $\lim_{r\to\infty} r_{app}^3[(q_t^3/q_0^3) - 1]$ can be represented as a converging series, where neglecting the higher order terms we get,

$$\lim_{r\to\infty} r_{app}^3\left[\left(q_t^3/q_0^3\right) - 1\right] = -3(1 - 1/q_0)\lim_{r\to\infty} r_{app}^3 f(r)$$

Again, assuming the following term to be a constant $k = \lim_{r\to\infty} r_{app}^3 f(r)/R^3$, the swelling deficiency for one particle is arrived at by replacing for q_t and k in Eq. (16),

$$\Delta v = \frac{4\pi q_0^3 R^3}{3}\left[\left(1 - 1/q_0^3\right)\left(1 + \varepsilon^2\right) - 3k(1 - 1/q_0)\right] \quad (17)$$

Presuming that within each unit volume of rubber the filler platelets are segregated in such a way that the filler–filler interactions are negligible, the swelling deficiency for all N particles can be designated as $\Delta V = N\Delta v$.

Also,

$$N = 3\phi/4\pi a^2 b(1 - \phi) \quad (18)$$

where, ϕ is the filler volume fraction and a and b are the major and minor axes of the ellipse representing the filler.

Thus, combining Eq. (17) and Eq. (18),

$$\Delta V = \frac{R^3}{a^2 b} q_0^3\left[\left(1 - 1/q_0^3\right)\left(1 + \varepsilon^2\right) - 3k(1 - 1/q_0)\right][\phi/(1 - \phi)] \quad (19)$$

The volume swelling ratios are inversely proportional to the equilibrium volume fraction of the rubber in the corresponding swollen systems (filled and gum), such that

$$Q/Q_0 = V_{r_0}/V_{r_f}, \quad 1/q^3 = v_r$$

Also,

$$Q/Q_0 = \left(q_0^3 + \Delta v\right)\Big/ q_0^3$$

From, Eq. (19),

$$Q/Q_0 = \frac{(q_0^3 + \Delta v)}{q_0^3} = 1 + \left[\left(1 - 1/q_0^3\right)\left(1 + \varepsilon^2\right) - 3k(1 - 1/q_0)\right] \times \frac{R^3}{a^2 b}[\phi/(1-\phi)]$$

Substituting for the equilibrium volume fraction we have,

$$V_{r_0}/V_{r_f} = 1 + \left[(1 - v_{r_0})\left(1 + \varepsilon^2\right) - 3k\left(1 - v_{r_0}^{1/3}\right)\right] \times \frac{R^3}{a^2 b}[\phi/(1-\phi)] = 1 - \left[3k\left(1 - v_{r_0}^{1/3}\right) + \left(1 + \varepsilon^2\right)v_{r_0} - \left(1 + \varepsilon^2\right)\right] \times \frac{R^3}{a^2 b}[\phi/(1-\phi)]$$

Factoring out $(1+\varepsilon^2)$ from above equation, we arrive at the final form

$$V_{r_0}/V_{r_f} = 1 - \left[\frac{3k\left(1 - v_{r_0}^{1/3}\right)}{(1+\varepsilon^2)} + v_{r_0} - 1\right]\frac{R^3}{a^2 b}\left(1 + \varepsilon^2\right)[\phi/(1-\phi)] \tag{20}$$

Thus, it is understood that V_{r_0}/V_{r_f} varies linearly, although not with $\phi/(1-\phi)$, but with a somewhat similar function which continues to bear the nanofiller's characteristic. In order to isolate the function, Eq. (20) is rearranged to get,

$$1 - V_{r_0}/V_{r_f} = \left[\frac{3k}{(1+\varepsilon^2)} - 1 - \frac{3k}{(1+\varepsilon^2)}v_{r_0}^{1/3} + v_{r_0}\right] \times \frac{R^3}{a^2 b}\left(1 + \varepsilon^2\right)[\phi/(1-\phi)]$$

or,

$$\frac{1 - V_{r_0}/V_{r_f}}{\left[\frac{3k}{(1+\varepsilon^2)} - 1 - \frac{3k}{(1+\varepsilon^2)}v_{r_0}^{1/3} + v_{r_0}\right]\frac{R^3}{a^2 b}\left(1 + \varepsilon^2\right)} = \phi/(1-\phi)$$

by substituting m' for the complex function below,

$$\left[\frac{3k}{(1+\varepsilon^2)} - 1 - \frac{3k}{(1+\varepsilon^2)}v_{r_0}^{1/3} + v_{r_0}\right]\frac{R^3}{a^2 b}\left(1 + \varepsilon^2\right) = m' \tag{21}$$

The above equation can be reduced to the form

$$\phi/(1-\phi) = \frac{1 - \left(V_{r_0}/V_{r_f}\right)}{m'}$$

or,

$$1/(1-\phi) = \frac{1 - \left(V_{r_0}/V_{r_f}\right)}{m'} + 1$$

The value of ϕ can be determined by taking the inverse of the above term and rearranging

$$(1-\phi) = m'\Big/\left[1 - \left(V_{r_0}/V_{r_f}\right) + m'\right]$$

Thus,

$$\phi = \left[1 - \left(V_{r_0}/V_{r_f}\right)\right]\Big/\left[1 - \left(V_{r_0}/V_{r_f}\right) + m'\right] \tag{22}$$

The original Kraus equation can be similarly rearranged to

$$\phi' = \left[1 - \left(V_{r_0}/V_{r_f}\right)\right]\Big/\left[1 - \left(V_{r_0}/V_{r_f}\right) + m\right] \tag{23}$$

where,

$$m = \left[3c - 1 - 3cv_{r_0}^{1/3} + v_{r_0}\right] \tag{24}$$

"c", defined as $c = \lim_{r\to\infty} r^3 f(r)/R^3$, is the constant analogous to "k" here.

On comparing these two equations, Eqs. (22) and (23), the presence of filler characteristics as additional terms in the expression for the slope is obvious. Thus, if a function has to accurately map the filler characteristics, it needs to be defined as the ratio of the two terms above, such that

$$\phi/\phi' = \psi = \left[1 - \left(V_{r_0}/V_{r_f}\right) + m\right]\Big/\left[1 - \left(V_{r_0}/V_{r_f}\right) + m'\right] \tag{25}$$

In an ideal case, when, $b = a = R$, so that $\varepsilon = 0$ and $d = k$, the equation we derived (Eq. (20)) reduces to the Kraus equation and so does the equation for the slope (Eq. (21)) to a form similar to that reported by Kraus (Eq. (24)) [6]. In the ideal case of the spherical filler embedment, the above function, ψ, equates to 1 (Eq. (25)).

Else,

$$\psi = \frac{1 - \left(V_{r_0}/V_{r_f}\right) + \left[3c - 1 - 3cv_{r_0}^{1/3} + v_{r_0}\right]}{1 - \left(V_{r_0}/V_{r_f}\right) + \left[\frac{3k}{(1+\varepsilon^2)} - 1 - \frac{3k}{(1+\varepsilon^2)}v_{r_0}^{1/3} + v_{r_0}\right]\frac{R^3}{a^2 b}\left(1 + \varepsilon^2\right)}$$

or, in terms of a and b,

$$\psi = \frac{1 - \left(V_{r_0}/V_{r_f}\right) + \left[3c - 1 - 3cv_{r_0}^{1/3} + v_{r_0}\right]}{1 - \left(V_{r_0}/V_{r_f}\right) + \left[\frac{3k}{\left(\frac{2a-b}{a}\right)} - 1 - \frac{3k}{\left(\frac{2a-b}{a}\right)}v_{r_0}^{1/3} + v_{r_0}\right]\frac{R^3}{a^2 b}\left(\frac{2a-b}{a}\right)} \tag{26}$$

The introduction of ϕ $(=\psi\phi')$ into to the original Kraus equation would thus incorporate the necessary amendment to accommodate the nanofiller characteristics. But, the function, ψ, thus arrived at is complicated and intractable because of the presence of the terms 'a', 'b' and 'k' (each of which is filler and system dependent) in it. Neglect of the additional terms in Eqs. (20) and (21) while drawing Kraus's plot would thus produce erroneous results. Hence it is required to replace the above function (Eq. (26)) with one comprising of known and easily measurable variables. This justifies our assumption that in the case of a platelet-like nanoparticle, represented here as an elliptical restraining feature, the available filler surface area at the interface and aspect ratio have a dominant role to play in the determination of the polymer–nanofiller interaction.

However, the aspect ratio determination for each particle in a polymer nanocomposite is impractical. It would require rigorous sample preparation, followed by transmission electron microscopy imaging and its complicated image analysis. It would also depend on the extent of exfoliation/intercalation achieved, which varies with the system and the processing conditions introduced, thereby preventing any attempt at generalizations.

Thus, a new function is required to accurately map the polymer–filler interactions in PNCs, which would adequately integrate all the dominant characteristics of the platelet-like nanofillers in the

nanocomposite. In accord with the above theory and the subsequent discussion, the polymer–nanofiller interaction parameter can be determined by introducing a new corrective function that is derived logically in the following section.

1.2. Derivation of the new corrective function

From the above discussion one can infer that certain assumptions made for obtaining Kraus's plot get violated in polymer nanocomposites having nanofillers, represented here by an elliptical shape. The shape and the aggregation effects of the nanofillers have not been duly accounted for in the Kraus plot. Also, after having meticulously deduced the expression for nanofillers (nanoclay, nanofiber, etc.), the assumption that the shape and the aggregation effects are included in the constant k would be a gross misappropriation. Hence, we logically deduce a corrective interface area function.

Since these nanofillers often have a rectangular shape, the elliptical shape assigned introduces some errors in calculation (Fig. 2). As illustrated in Fig. 2, the ellipse having major axis 'a' and minor axis 'b', which can map the platelet-like nanofiller, would have a deficit of $(4-\pi)$ in the interfacial area per particle. This is the difference between the rectangular area ($4ab$) and that of the ellipse (πab). However, it needs appreciation that as the aspect ratio increases the ellipse attains a rectangular shape, which would eventually almost eliminate the difference in areas. Thus, while attempting to derive the new function it is realized that a correction factor corresponding to the interface area needs to be introduced. The discrepancy due to shape and the aggregation effects can be addressed by introducing an interfacial area function. The shape factor can be resolved by introducing the aspect ratio. But as its accurate measurement in the nanocomposite is rigorous and error prone, we introduce the filler density (ρ) and its specific surface area (ζ) to address the shape factors. This can successfully represent the aspect ratio effects because changes in aspect ratio are reflected in the ratio of particle surface area to particle volume, that is, density $\times$ surface area/g.

Also, the loss in available surface area due to overlapping and aggregation is quite substantial in the case of nanofiller. As illustrated in Fig. 3, it is directly dependent on the interparticle distance between the fillers and hence also on the filler loading. We propose the introduction of these two terms in the form of the correlation length between the nanoparticles (ξ) and the filler volume fraction (ϕ), respectively, to the interfacial area function.

The interface area function (IAF) is thus designed to represent the filler characteristics, $\{R^3(1+\varepsilon^2)/a^2b\}$, that surfaced in Eq. (20) and those inseparable from the expression for the slope (Eq. (21)). Thus, the corrective function, ψ (IAF), introduced to accommodate the shape and aggregation effects can be defined as

$$\psi = \rho\cdot\zeta\cdot\xi\cdot\phi \tag{27}$$

This customized function also circumvents the intractability problem pertinent to Eq. (26). Unlike the area function discussed previously to relate the physical properties of carbon black to the overall viscoelastic properties of the composite [21], the function introduced here is unique because it is a dimensionless quantity. Thus, it would be able to better represent the property without any significant bias arising out of the differences in magnitudes of the constituting components.

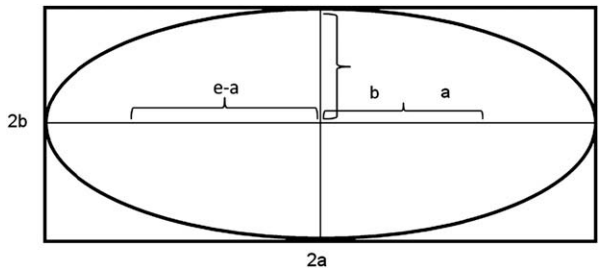

Fig. 2. Comparing the elliptical shape against its enclosing rectangular shape.

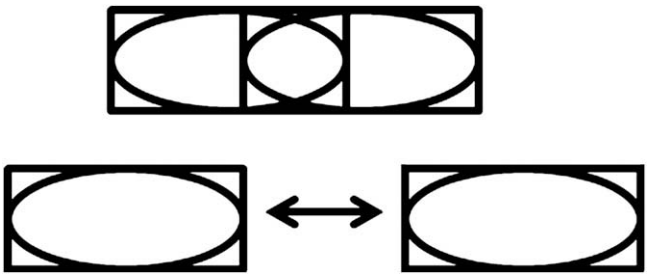

Fig. 3. Depiction of change in available and lost surface due to differing correlation length.

It can be concluded that, the IAF which reflects the surface energy, aspect ratio, nanofiller content and also, the dispersion of the nanofillers in the nanocomposite would hence successfully map the filler characteristics in the nanocomposite to reduce Eq. (20) into the original Kraus form, where $\phi = \psi\phi'$.

Thus, the modified Kraus equation can be represented as,

$$V_{r_0}/V_{r_f} = 1 - m[\psi\phi/(1-\psi\phi)] \tag{28}$$

where, ψ is the new Interface Area Function (IAF).

These observations are compiled to tailor the Halpin–Tsai equation into a much simpler form for PNCs comprising of matrix–filler combinations having inordinately disparate sets of Young's moduli. This was done by addressing the shape, size and aggregate related factors *a priori* to adequately supplant those in Eq. (3). For rubber–clay system, $E_f \gg E_m$. Therefore, $(E_f/E_m) - 1 \approx (E_f/E_m) + \xi \approx E_f/E_m$, and $\eta \approx 1$. This reduces the Halpin–Tsai equation (Eq. (3)) into

$$E = E_m\left\{\frac{1+2\alpha\phi}{1-\phi}\right\} \tag{29}$$

As seen, Halpin–Tsai equation has a term α, raised to the power of one, to accommodate the filler aspect ratio. Since our function intends to supplant the same, the new equation is expected to have a reduced dependence on the aspect ratio. This understanding is subjected to test by sequentially diluting the presence of aspect ratio in the equation. The first modified Halpin–Tsai equation contains a correction term in the form of a shape reduction factor ($\alpha^{0.5}$), Eq. (30), while the second modified Halpin–Tsai equation, Eq. (31), is devoid of any extra shape related corrections.

Modified Halpin–Tsai I,

$$E = E_m\left\{\frac{1+\alpha^{0.5}\psi\phi}{1-\psi\phi}\right\} \tag{30}$$

and modified Halpin–Tsai II,

$$E = E_m\left\{\frac{1+\psi\phi}{1-\psi\phi}\right\} \tag{31}$$

2. Experimental

2.1. Materials

Natural rubber, (Mooney Viscosity, $ML_{1+4} = 60$ at 100 °C) was supplied by the Rubber Board, Kottayam, Kerala, India. Styrene butadiene rubber, (SBR-1502, Mooney Viscosity, $ML_{1+4} = 53$ at 100 °C and bound styrene content of 23.5%) was procured from Korea Kumho Petrochemical Co. Ltd., Seoul, Korea.

Table 1
Formulation of the mix used

Ingredient	Loading (wt. phr)	Loading (vol. phr)
Rubber	100.0	100.0
Zinc oxide	5.0	0.84
Stearic acid	2.0	2.21
IPPD	1.0	0.89
Sulphur	2.0	0.91
CBS	0.8	0.50

The fillers used were organomodified clays – Cloisite 15A (Montmorillonite clay from Southern clay products, USA) and Pangel B20 (Sepiolite clay from Tolsa S.A., Spain) – and carbon nanofiber, Pyrograf-III, PR-24 (Vapour Grown Carbon Fiber from Pyrograf® Products, Inc., USA).

Standard rubber grade zinc oxide, sulphur, benzene and toluene were procured from Merck Ltd., Mumbai, India. Stearic acid was supplied by Shreeji Fine Chemicals, Mumbai, India and *N*-cyclohexyl-2-benzothiazyl sulfenamide (CBS) by ICI India Ltd., Chemicals Division, Mumbai, India. *N*-Isopropyl-*N*′-phenyl-*p*-phenylenediamine (IPPD) was provided by Bayer Chemicals AG (presently, Lanxess), Leverkusen, Germany. Ethanol was procured from Bengal Chemicals and Pharmaceuticals Ltd., Kolkata, India.

The formulation used in this investigation is tabulated in Table 1. The basic formulation was kept common for all the systems. There was no variation in the loading of anti-oxidant, curatives and cure accelerators.

The samples and their designations are illustrated in Table 2.

2.2. Preparation of nanocomposites

The nanofiller was initially mixed with the rubber in a Brabender Plasticorder (PLE 330) at 80 °C at 60 rpm for 2 min. The remaining compounding ingredients, except the curative package, were then added and mixed in the Brabender under the above mentioned conditions for 3 min. The curatives were subsequently added to the resulting masterbatch in a two-roll mill (Schwabenthan, Berlin), following standard mixing sequence. The filler loading was varied from 2 phr till the loading at which saturation of mechanical properties was observed. This has been discussed in our previous reports [22,23].

The optimum cure time of the mixes was obtained from a Monsanto Oscillating Disc Rheometer (ODR-100s) in accord with ASTM D 2084-93. The tensile slabs were prepared by curing till optimum cure time at 150 °C in a David-Bridge hydraulic press (supplied by Castleton, Rocchdle, England) at a pressure of 5 MPa. The specimens were conditioned at room temperature for 16 h before carrying out the testing.

2.3. Swelling studies

The cured samples were separately immersed in benzene and toluene for 48 h at an ambient temperature of 25 °C. The equilibrium volume fraction of rubber in the swollen gel was also calculated using the following equation [24].

$$V_r = \frac{(D - FT)\rho_r^{-1}}{(D - FT)\rho_r^{-1} + A_0\rho_s^{-1}} \quad (32)$$

where, D = Deswollen weight, F = weight fraction of the insoluble component, T = initial weight of the test specimen, ρ_r = density of rubber, ρ_s = density of solvent, A_0 = amount of solvent absorbed.

Table 2
Filler loading and corresponding sample designation

Rubber	NR			SBR		
Filler[a]/loading (phr)	15A	SP	F	15A	SP	F
2	N15A2	NSP2	NF2	S15A2	SSP2	SF2
4	N15A4	NSP4	NF4	S15A4	SSP4	SF4
6	N15A6	NSP6	NF6	S15A6	SSP6	SF6
8	–	–	–	S15A8	–	–

[a] Cloisite 15A (15A), Pangel B20 (SP), Pyrograf-III (F).

2.4. Tensile properties

Tensile specimens were punched out from the molded sheets using ASTM Die-C. The tests were carried out as per the ASTM D 412–98 method in a Universal Testing Machine (Zwick Z010) at a cross-head speed of 500 mm/min at 25 ± 2 °C. Young's modulus was calculated from the slope of the tensile curve in the linear region (upto 30% elongation). The average of three tests is reported here for the modulus.

2.5. Transmission electron microscopy (TEM)

The nanocomposite samples for TEM analysis were prepared by ultra cryomicrotomy using Leica Ultracut UCT, at around 40 °C below the glass transition temperature (T_g) of the compounds. Freshly cut glass knives with cutting edge of 45° were used to get the cryosections of 50 nm thickness. The microscopy was performed using JEOL-2100 electron microscope, having LaB_6 filament, operating at an accelerating voltage of 200 kV. Image analysis of the bright field images was performed using UTHSCSA Image Tool for Windows Version 3.00. It was used to determine the correlation length used in the newly introduced interface area function.

2.6. Surface energy

The surface energy of the solid polymers was determined by contact angle measurement, while that of the nanofillers was determined using Washburn and Fowkes equations. The theory, procedural details and references, along with the results have been discussed in our earlier papers [22,23].

3. Results

The density and specific surface area for the fillers and the nanocomposites are tabulated in Table 3. The N_2 surface area values have been earlier reported in the literature [25–27] and the density was taken from the material data sheets of the respective fillers. The correlation length was determined from image analysis of the TEM pictures of the respective nanocomposites, which have been reported in our earlier reports [22,23,28].

The modified Kraus plots for the three sets of fillers are shown in Fig. 4a–d. Fig. 4a and b corresponds to the swelling studies of the natural rubber (NR) and styrene–butadiene rubber (SBR) PNCs, respectively, in benzene. Fig. 4c and d is the analogous modified Kraus plot using toluene as the swelling solvent. The lines drawn are the best fit lines of the corresponding scatter points of the experimental data sets. The slopes of the modified Kraus plots and

Table 3
Interfacial area parameters for the different fillers

	Density[a] (gm/cm^3)	N_2 surface area[b] (m^2/gm)
Cloisite 15A	1.66	147 [25]
Pangel B20	2.10	364 [26]
Pyfrograf-III, PR-24	1.95	60 [27]

[a] Density values have been quoted from respective supplier's MSDS.
[b] Total specific surface area (BET surface area) values for the respective nanofillers.

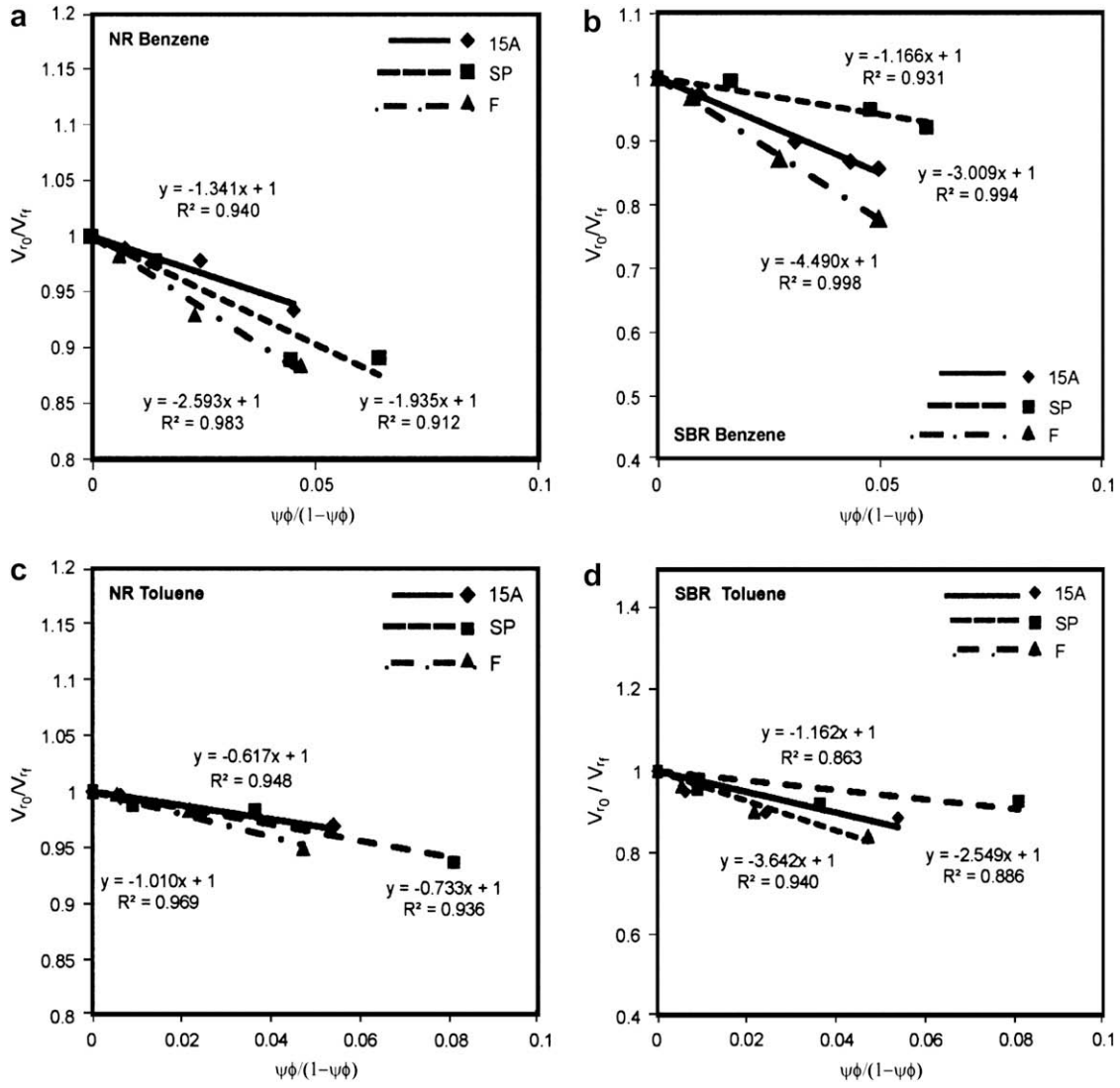

Fig. 4. Modified Kraus plots for the three sets of filler for (a) NR and (b) SBR swollen in benzene. Modified Kraus plots for the three sets of filler for (c) NR and (d) SBR swollen in toluene.

their corresponding coefficient of determination are listed in Table 4. Swelling studies done in both benzene and toluene (Fig. 4a and b) conform the modified Kraus equation. The high regression coefficients imply that IAF successfully represents the nanocomposite properties.

The universal applicability of IAF is also demonstrated by introducing it into a fluoroelastomer–Cloisite NA polymer nanocomposite, reported earlier from our laboratory [28]. Fig. 5 displays the modified Kraus plot for the fluoroelastomer nanocomposite. A linear fit is observed with a relatively high regression coefficient value of the best fit line, shown in the graph.

These results indicate both the necessity and efficacy of the interface area function in understanding the polymer–nanofiller interaction parameter. It also justifies the approach undertaken to identify the possible constituents of this function, specifically for platelet type nanofiller filled polymer nanocomposites.

Fig. 6a–d is the Kraus plot for the three sets of fillers. Fig. 6a and b corresponds to the swelling studies of the NR PNCs in toluene and benzene, respectively. Fig. 6c and d is the analogous Kraus plot for the SBR PNCs. Kraus plot not only exhibits lower regression coefficients of the best fit lines, but also in the case of NR it erroneously predicts a stronger polymer–nanofiller interaction with sepiolite, in comparison with carbon nanofiber (discussed later). The slope of the Kraus plots and their corresponding coefficient of determination are listed in Table 5. It is seen that there exist some discrepancies in the results of the Kraus plot, if they were to be correlated to the surface energy data.

We have extended the purview of our interface area function, by using it to determine Young's modulus since it is expected to bear direct effect on the mechanical properties of the nanocomposites.

Table 4
Slope of the modified Kraus plots and their corresponding coefficient of determination

	NR				SBR			
	Slope, m		Coefficient of determination, R^2		Slope, m		Coefficient of determination, R^2	
Filler	Bz	To	Bz	To	Bz	To	Bz	To
15A	1.34	0.62	0.940	0.948	3.00	2.55	0.994	0.886
SP	1.94	0.73	0.912	0.936	1.17	1.16	0.931	0.863
F	2.59	1.01	0.983	0.969	4.49	3.64	0.998	0.940

Bz = benzene, To = toluene.

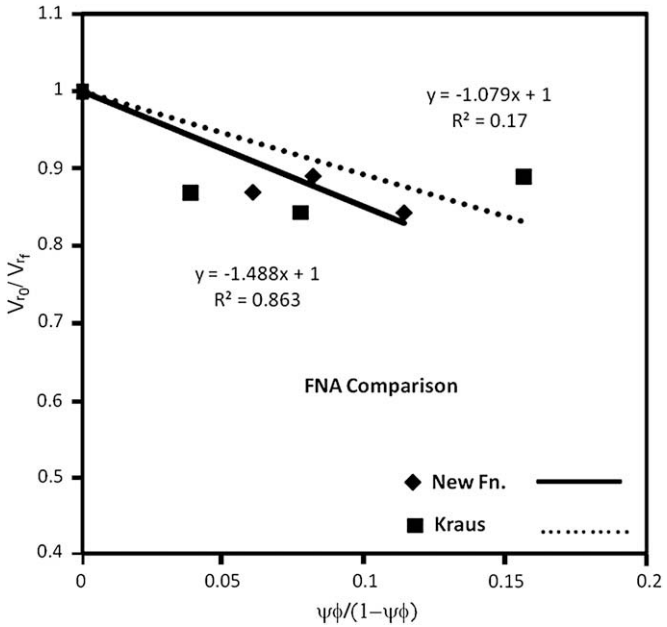

Fig. 5. Modified (New fn.) and the unmodified Kraus plots for the Cloisite NA filled fluoroelastomer nanocomposite.

We have introduced the IAF in the Guth–Gold (Eq. (1)), modified Guth–Gold (by Guth, Eq. (2)), Halpin–Tsai (Eq. (3)) and some variants of modified Halpin–Tsai equations (Eqs. (30) and (31)) to account for the contribution of the platelet-like filler to Young's modulus in polymer nanocomposites.

Fig. 7a–c (for NR) and Fig. 8a–c (for SBR) show the experimental data along side the data predicted using the above equations. The line is the best fit line of the experimental data, while the scatter points are the corresponding values predicted using the various equations as indicated by their respective legends in the graph. Guth–Gold (Eq. (1)), modified Guth–Gold (by Guth, Eq. (2)), Halpin–Tsai (Eq. (3)) and modified Halpin–Tsai (Eqs. (30) and (31)) equations have been plotted after the introduction of IAF into them. Young's modulus was calculated from the slope of the tensile curve in the linear region (upto 30% elongation). The error is within 2–4% and hence the error bars are not visible. The scatter points are, however, unique values predicted by the modified equations, and hence do not bear error bars.

Table 6 compiles the percent average deviations of the values predicted by the various constitutive equations studied post-introduction of the IAF. It is observed from the deviation data (Table 6) that predictions by even the simple Guth–Gold equation (Eq. (1)) derived for spherical fillers are quite accurate, whereas the complex equations {modified Guth–Gold (by Guth, Eq. (2)) and Halpin–Tsai (Eq. (3))} containing shape factor and other similar parameters give exceedingly large deviations (Figs. 7 and 8). The deviation in the case of Guth–Gold equation is 9–19% while those for modified

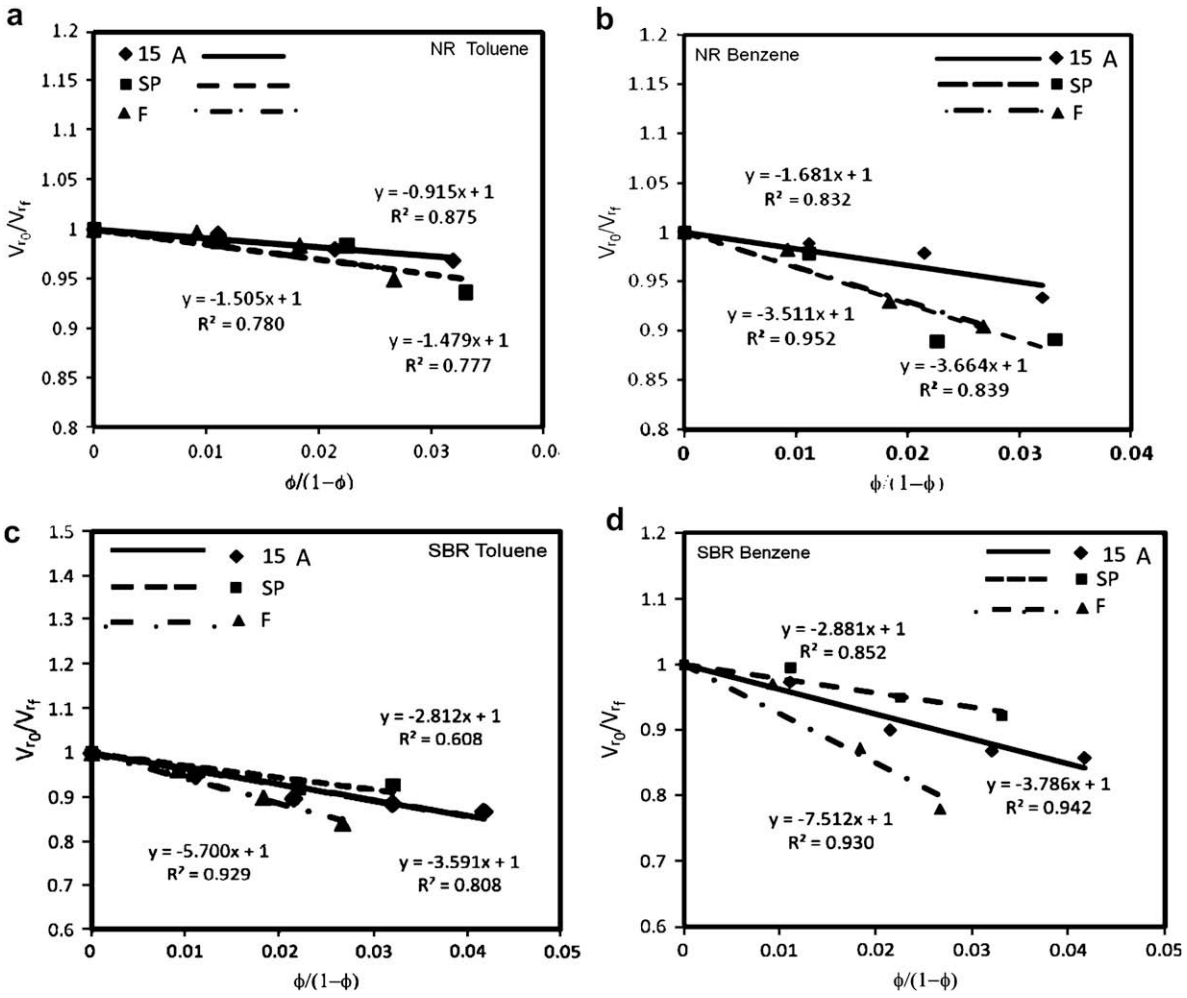

Fig. 6. Kraus plots for the three sets of NR-filler nanocomposites swollen in (a) toluene and (b) benzene. Kraus plots for the three sets of SBR-filler nanocomposites swollen in (c) toluene and (d) benzene.

Table 5
Slope of the Kraus plots and their corresponding coefficient of determination

	NR				SBR			
	Slope, m		Coefficient of determination, R^2		Slope, m		Coefficient of determination, R^2	
Filler	Bz	To	Bz	To	Bz	To	Bz	To
15A	1.68	0.92	0.832	0.875	3.79	3.59	0.942	0.808
SP	3.64	1.52	0.839	0.780	2.88	2.81	0.852	0.608
F	3.51	1.48	0.952	0.777	7.51	5.71	0.930	0.929

Bz = benzene, To = toluene.

Guth–Gold and Halpin–Tsai are 248% and 265%, respectively, due to the above mentioned factors.

Even without the introduction of the correction factor, the Guth equation per se gives error in prediction as high as 17–35%, in the case of the nanocomposites studied. The modified Guth–Gold and Halpin–Tsai equations too are found to be error prone, with 21–101% and 29–107% error in prediction. These errors increase continually with nanofiller loading.

The close fit of the experimental data and the values predicted by the constitutive modified Halpin–Tsai equations I and II (Eqs. (30) and (31)), as seen in Fig. 7a–c (for NR) and Fig. 8a–c (for SBR), illustrates the just definition of the IAF. Table 6 also confirms that newly devised equations, (Eqs. (30) and (31)), provide astounding results since their predictions conform to the experimental data.

4. Discussion

Conventionally, polymer–filler interaction has been studied using the Kraus plot, the slope of which indicates the measure of the interaction. The greater the magnitude of the slope, the higher is the interaction. Kraus had derived the system by considering the restriction to swelling caused by spherical filler. The nanofillers, the nanoclay in particular, are not spherical. In fact they are platelet-like in terms of their structure. On introduction of the interface area function (IAF) to the erstwhile Kraus equation, it is seen that the order of the polymer–nanofiller interaction of nanocomposites as determined from the swelling experiments (Figs. 4a–d and 5) also agrees with the trends in the modulus (Figs. 7 and 8), shown in the previous section. Also, the coefficients of determination values of the best fit lines of the corresponding swelling studies (Table 4) are satisfactory, as well. In order to determine the suitability of IAF, the volume swelling studies were carried out by using two different swelling solvents, benzene and toluene, for both NR and SBR. The better fit observed in the case of benzene is because it has closer values of Flory–Huggins parameter for NR (0.435) and SBR(0.398), than the corresponding values of 0.420 and 0.280 in the case of toluene.

The above observations made on a large number of rubber–nanofiller and nanocomposite-swelling solvent systems highlight that the amendment of the Kraus plot by the introduction of the interface area function (IAF) renders the plot applicable to PNCs.

It can be inferred from Fig. 6a–d and Table 5 that the Kraus plot should be adequately modified for accurate determination of the

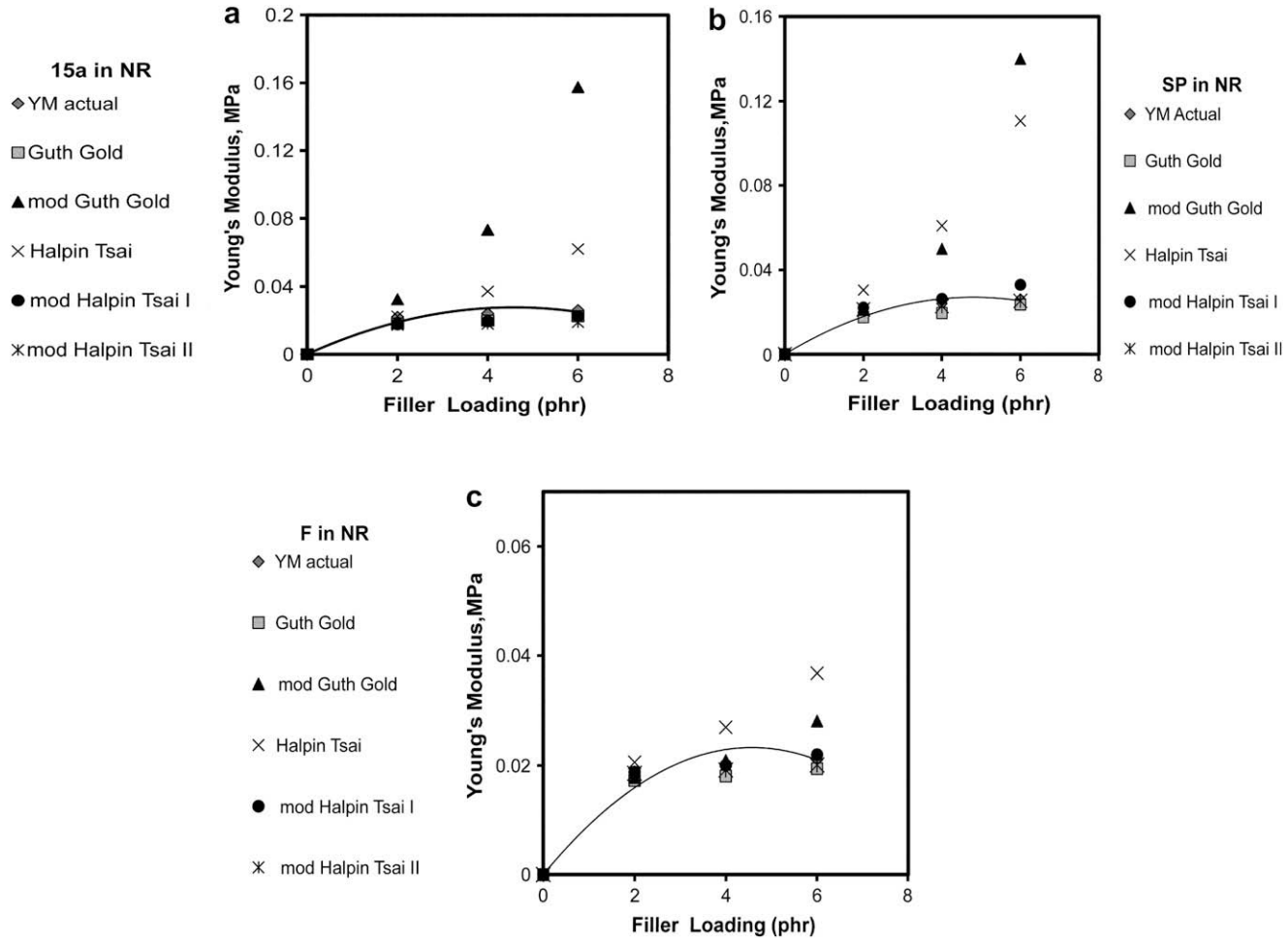

Fig. 7. Fitment of composite models on introduction of IAF, for the (a) Cloisite 15A, (b) sepiolite and (c) carbon nanofiber filled NR nanocomposites; YM = Young's modulus.

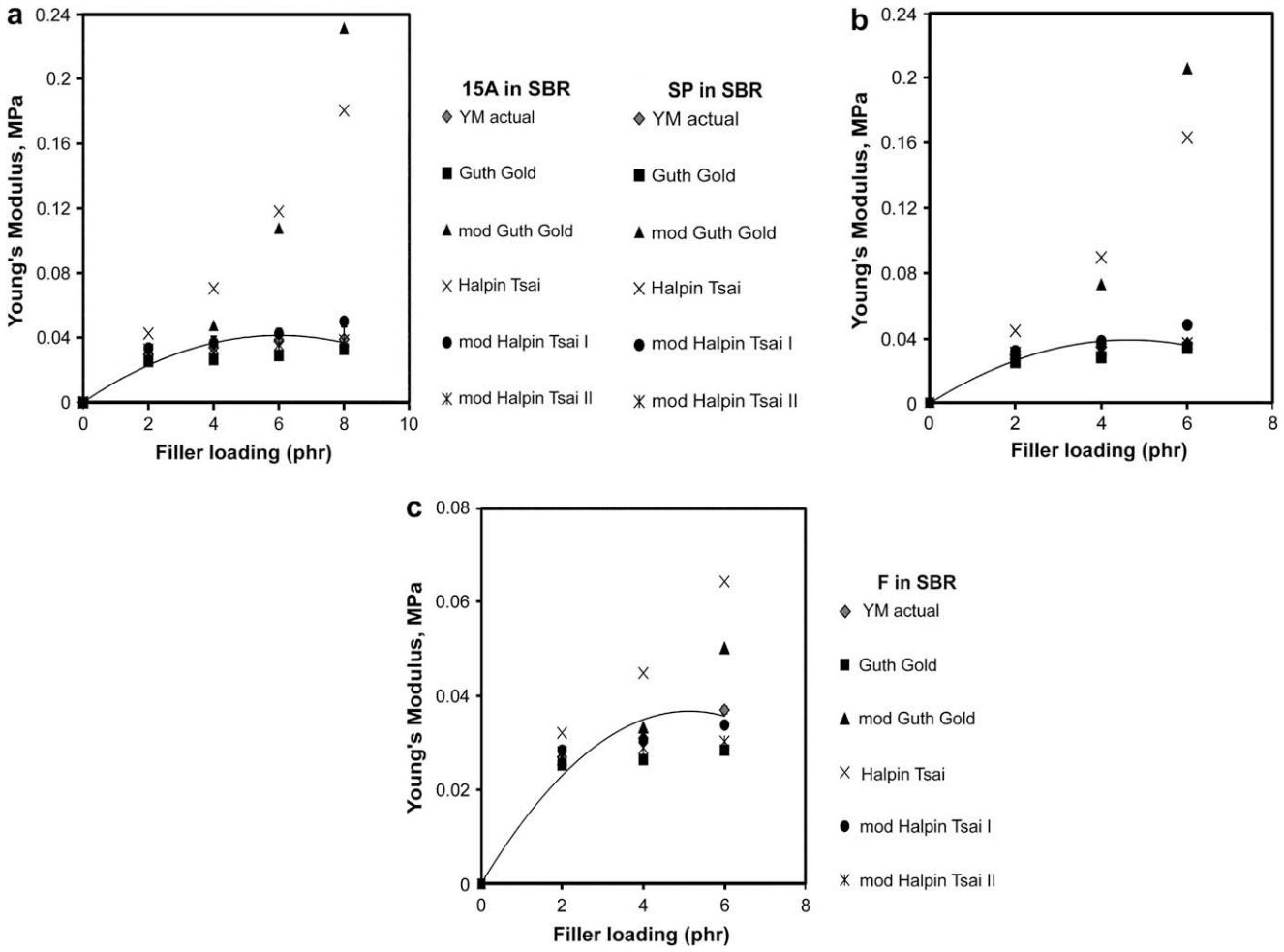

Fig. 8. Fitment of composite models on introduction of IAF, for the (a) Cloisite 15A, (b) sepiolite and (c) carbon nanofiber filled SBR nanocomposites; YM = Young's modulus.

polymer–nanofiller interaction parameter. Here, the coefficients of determination are significantly less than unity. In terms of statistics it means that although the present function relating the independent variable to the dependent variable is robust, its accuracy of mapping is hindered possibly because of neglecting certain other parameters which influence the independent variable.

Further, some discrepancies in determining the trend amongst the different nanofillers, especially in the case of natural rubber (Fig. 6a and c) systems are observed in the Kraus plot. The plots suggest that the interaction parameter would follow the order: sepiolite > carbon nanofiber > Cloisite 15A. Following Zisman approach, the trend for polymer–nanofiller interaction is expected to be decisively in favour of carbon nanofiber by virtue of its higher surface energy (Table 7). This, however, is not reflected in the case of NR (Fig. 6a and c). Thus, we can infer that Kraus plot fails to display the right trend.

The extent of polymer–nanofiller interaction is in essence determined by the respective characteristic surface energies of the polymer and the nanofiller. From Zisman approach, the higher the filler surface energy, the higher is its wettability by the polymer. Such wetting is characterized by a high work of adhesion (W_a) and positive spreading coefficient value. On the other hand, poorly wet interfaces are indicated by low W_a and negative spreading coefficients.

The other determining feature is the interparticle cleavage energy. However, it is extremely difficult to measure for nanofillers. On cleavage if a mineral undergoes minimal surface reconstruction, the surface tension can be treated as the free energy of cleavage which suggests a small entropic contribution, and hence correlating it further to the cleavage energy [29].

We have already discussed in detail the implications of surface energy (and its various components), the W_a and cleavage energy in both SBR [22] and NR [23] systems that we have studied.

Table 6
Percent average deviations of the various constitutive equations, after introduction of the IAF

Filler	15A		SP		F	
Model	NR	SBR	NR	SBR	NR	SBR
Guth–Gold	16	19	14	13	9	15
Modified Guth–Gold	248	178	184	190	14	15
Halpin–Tsai	265	181	177	182	44	46
Modified Halpin–Tsai I	17	15	15	16	5	2
Modified Halpin–Tsai II	25	0	1	0	0	7

Table 7
Contact angle and surface energy of the rubbers and the fillers

Sample	Contact angle (°)		γ (mJ/m^2)	γ_s^d (mJ/m^2)	γ_s^p (mJ/m^2)
	Water	Formamide			
NR	100	71	35.10	34.99	0.12
SBR	71	61	33.17	16.07	17.10
Cloisite 15A	88	84	19.37	6.98	12.39
Sepiolite	67	52	38.26	21.53	16.73
C-Fiber	78	48	44.01	39.79	4.22

Table 7 lists the surface energy (SE) and its two components for the two rubbers and the three nanofiller systems which have been the focus of our studies. Following Zisman approach, the surface energy data would suggest that the order of wetting of filler by polymer and hence, the polymer–nanofiller interaction should be: carbon fiber > sepiolite > Cloisite 15A.

This would have been true if the fillers were morphologically same, which they are not. Sepiolite is a non-expandable clay with narrow channels along the fiber axis which are densely populated with highly active Si–OH groups at their edges. Thus it has equitable contributions from the polar and the dispersive components to its surface energy. Cloisite (MMT) is expandable clay of plain layered structure with very few exposed Si–OH groups, that too at the edges of the very end of each platelet. Cloisite 15A has the highest (36%) modifier content amongst modified clays of its kind, and hence demonstrates a precipitous drop in its observed surface energy value. Carbon fiber eponymic to its name has long cylindrical fibrous structure with very few surface active groups.

Thus, carbon fiber having 16% higher SE than sepiolite would be expected to demonstrate maximum wetting, followed by sepiolite and Cloisite 15A. The order in fact remains so for natural rubber (NR), which has linear chains that get accommodated in the narrow channels in sepiolite's structure. However, as discussed earlier [22], for styrene–butadiene rubber (SBR) the order is altered a bit. This can be attributed to the reduced penetration of the macromolecular chains into sepiolite's channels because of the bulky styrenic side-chain substitutions, as compared to the linear NR chains.

Thus, taking into account the surface energy and morphological parameters the expected order for polymer–filler interaction is NR: carbon nanofiber > sepiolite > Cloisite 15A. SBR: carbon nanofiber > Cloisite 15A > sepiolite.

This is indeed reflected in the trends in the mechanical property enhancements [22,23], but not in the Kraus plot results, which erroneously suggest that for NR, the interaction parameter would follow the order: sepiolite > carbon nanofiber > Cloisite 15A.

In order to account for these anomalies in the Kraus plot results, we derived the interface area function which incorporates the effects of the filler size, shape and also the correlation length, which is known to influence polymer nanocomposite properties strongly [30,31].

In the interface area function (IAF), the aspect ratio of the nanofillers in the nanocomposites is correlated with the specific surface area, as explained earlier. Since actual measurement of thickness of the nanofiller (which is around 1–10 nm) is tedious and error prone, the sampling errors are minimized by introducing the characteristic correlation length instead. Correlation length (which is at least 100 nm for most nanocomposites) was determined by statistically analyzing TEM micrographs. The introduction of IAF imparts definitive change to the predicting ability of the constitutive equations for polymer–filler nanocomposites (Figs. 7 and 8) and Table 6.

These observations further support our approach in evolving the new IAF and the ability of its constituents to correctly represent the shape and aggregate parameters. This is underlined by the fact that even the Guth–Gold equation on introduction of our IAF predicts Young's modulus with a great degree of accuracy. On the other hand, the pre-incorporation of shape related factors in the IAF causes a multiplicative term to be carried through in the case of modified Guth–Gold and Halpin–Tsai equations. Since these equations already have shape related correction introduced (to address rod-like fillers, instead of spherical fillers) the inclusion of IAF results in gross over estimation, especially at higher loadings of nanofillers with high specific surface areas.

5. Conclusions

For polymer nanocomposites, the polymer–nanofiller interaction parameter has seldom been studied in terms of the Kraus plot. In fact its viability too has not been studied. On attempting that we observe certain discrepancies in trend depiction *vis-à-vis* that expected from surface energy data. Also, the plots are plagued by low regression coefficient values.

On modifying the basic tenet by substituting the spherical inclusion with an elliptical platelet-like restraining body it is found that certain terms characteristic of nanofillers surface in the equation. It signifies the need of a correction factor which is incorporated in the form of an interface area function (IAF). This correction factor comprising of the specific surface area, correlation length between nanofillers in the composite and the filler volume fraction results not only in better fitment, indicated by higher regression coefficients, but also conformance with the trend predicted by surface energy data.

The accurate representation of the polymer–nanofiller interaction by the IAF is also highlighted by the improvement in the predictive capabilities of simple composite models, the Guth–Gold equation, on its introduction. Since the IAF suitably integrates the shape and aggregate effects in PNCs, it was applied to tailor the Halpin–Tsai equation into much simpler forms for PNCs comprising of matrix–filler combinations having extremely large difference in Young's moduli. Unlike original Halpin–Tsai equations, these were able to predict the composite's Young's modulus within acceptable limits, which further underline the necessity of inclusion of IAF and the justification in choosing its constituents.

Acknowledgment

We gratefully acknowledge Mr. Sachin Shaw of Indian Institute of Technology Kharagpur, India, for his assistance in this work.

References

[1] Flory PJ, Rehner Jr J. J Chem Phys 1943;1:521.
[2] Bueche AM. J Polym Sci 1955;15:97.
[3] Kraus G. Rubber World 1956;135(67):254.
[4] Boonstra BBS, Dannenberg EM. Rubber Age 1958;82:838.
[5] Lorenz O, Parks CR. J Polym Sci 1961;50:299.
[6] Kraus G. J Appl Polym Sci 1963;7:861.
[7] Fornes TD, Paul DR. Polymer 2003;44:4993.
[8] Brune DA, Bicerano J. Polymer 2002;43:369.
[9] Shia D, Hui CY, Burnside SD, Giannelis EP. Polym Compos 1998;19:608.
[10] Bandyopadhyay A, De Sarkar M, Bhowmick AK. J Polym Sci Part B Polym Phys 2005;43:2399.
[11] Sadhu S, Bhowmick AK. Rubber Chem Technol 2005;78:321.
[12] Datta H, Singha NK, Bhowmick AK. Macromolecules 2008;41:50.
[13] Maiti M, Bhowmick AK. Polymer 2006;47:6156.
[14] Ganguly A, De Sarkar M, Bhowmick AK. J Appl Polym Sci 2006;100:2040.
[15] Sengupta R, Bandyopadhyay A, Sabharwal S, Chaki TK, Bhowmick AK. Polymer 2005;46:3343.
[16] Guth E, Gold O. Phys Rev 1938;53:322.
[17] Guth E. J Appl Phys 1945;16:20.
[18] Halpin JC, Kardos JL. Polym Eng Sci 1976;16:344.
[19] Halpin JC. J Compos Mater 1969;3:732.
[20] Nielsen LE. J Appl Phys 1970;41:4626.
[21] Caruthers JM, Cohen RE, Medalia AI. Rubber Chem Technol 1976;49:1076.
[22] Bhattacharya M, Maiti M, Bhowmick AK. Polym Eng Sci, in press. doi:10.1002/pen.
[23] Bhattacharya M, Maiti M, Bhowmick AK. Rubber Chem Technol, in press. For tentative publication in NOV/DEC issue 2008.
[24] Bhowmick AK, Mangaraj D. In: Bhowmick AK, Hall MM, Benarey H, editors. Rubber products manufacturing technology. New York: Marcel Dekker; 1994. p. 363.
[25] Grillet Y, Cases JM, Francois M, Rouquerol J, Poirier JE. Clays and Clay Minerals 1988;36:233.
[26] Aylmore LAG, Sills ID, Quirk JP. Clays and Clay Minerals 1970;18:91.
[27] http://www.apsci.com/ppi-pyro3.html; 2007 [accessed 20.09.07].
[28] Maiti M, Bhowmick AK. J Polym Sci Part B Polym Phys 2006;44:162.
[29] Heinze H, Vaia RA, Farmer BL. J Chem Phys 2006;124:224713.
[30] Ray SS, Okamoto M. Prog Polym Sci 2003;28:1539.
[31] Sheng N, Boyce MC, Parks DM, Rutledge GC, Abes JI, Cohen RE. Polymer 2004;45:487.